A Point Mutation in *PDGFRB* Causes Autosomal-Dominant Penttinen Syndrome

Jennifer J. Johnston,[1,6] Monica Y. Sanchez-Contreras,[2,6] Kim M. Keppler-Noreuil,[1] Julie Sapp,[1] Molly Crenshaw,[1] NiCole A. Finch,[2] Valerie Cormier-Daire,[3] Rosa Rademakers,[2] Virginia P. Sybert,[4,5,7] and Leslie G. Biesecker[1,7,*]

Penttinen syndrome is a distinctive disorder characterized by a prematurely aged appearance with lipoatrophy, epidermal and dermal atrophy along with hypertrophic lesions that resemble scars, thin hair, proptosis, underdeveloped cheekbones, and marked acro-osteolysis. All individuals have been simplex cases. Exome sequencing of an affected individual identified a de novo c.1994T>C p.Val665Ala variant in *PDGFRB*, which encodes the platelet-derived growth factor receptor β. Three additional unrelated individuals with this condition were shown to have the identical variant in *PDGFRB*. Distinct mutations in *PDGFRB* have been shown to cause infantile myofibromatosis, idiopathic basal ganglia calcification, and an overgrowth disorder with dysmorphic facies and psychosis, none of which overlaps with the clinical findings in Penttinen syndrome. We evaluated the functional consequence of this causative variant on the PDGFRB signaling pathway by transfecting mutant and wild-type cDNA into HeLa cells, and transfection showed ligand-independent constitutive signaling through STAT3 and PLCγ. Penttinen syndrome is a clinically distinct genetic condition caused by a *PDGFRB* gain-of-function mutation that is associated with a specific and unusual perturbation of receptor function.

There is a group of genetic conditions, including Hutchinson-Guilford (progeria) syndrome (MIM: 176670), Wiedemann-Rautenstrauch syndrome (MIM: 264090), mandibuloacral dysplasia (MIM: 248370), Nestor-Guillermo syndrome (MIM: 614008), Cockayne syndrome (MIM: 216400), xeroderma pigmentosum groups A–G (MIM: 278700, 610651, 278720, 278730, 278740, 278760, 278780, and 278750), and Werner syndrome (MIM: 277700), with features that resemble premature aging. Hutchinson-Guilford progeria manifests in premature death due to atherosclerosis and renal failure. Other disorders, such as Werner syndrome, Cockayne syndrome, and xeroderma pigmentosum, primarily cause premature death by cancer susceptibility and are caused by defective DNA repair. A number of disorders have some attributes of premature aging without premature death and are termed "progeroid" disorders. A disorder originally described as a "new progeroid disorder" (MIM: 601812) was delineated in 1997 by Penttinen et al.[1] in a child with thin and sparse hair, subcutaneous lipoatrophy, sclerotic skin lesions, and acro-osteolysis, among other features. A subsequent individual was described by Zufferey et al.[2] We identified two additional individuals with this distinctive phenotype and performed clinical characterization and molecular analysis by exome sequencing and functional analysis of the altered protein. Insight into important biological processes can be gained by understanding the molecular and pathophysiologic basis of these disorders.

All individuals in this study provided written informed consent and the National Human Genome Research Institute (NHGRI) institutional review board (IRB) reviewed and approved this study. This study was performed under NHGRI-IRB-approved protocols 10-HG-0065 and 94-HG-0193.

Individual 1 was originally reported by Penttinen et al.[1] He was of Finnish descent, the second child born to healthy parents, was first seen at 3 years of age, and was described as having a "senile" appearance, scar-like skin nodules on the hands and feet, corneal clouding, and a red reticular rash on his cheeks. Between 6 and 8 years, he was diagnosed with mild sensorineural hearing loss, hypothyroidism (which his family history is positive for), hyperopia, and poor weight gain. At 10 years, he was noted to have hyperextensible knees and elbows and a "prematurely aged appearance," along with an increase in the distribution and size of the skin nodules on the hands, feet, knees, and elbows. Biopsy of a nodule showed deposition of periodic acid-Schiff (PAS)-stain-negative material in the dermis. His intelligence was reported to be normal. He has had multiple fractures and scoliosis that required surgical instrumentation placement, and he receives annual intravenous zolendonric acid treatment for osteoporosis.

On evaluation at the age of 29 years, his weight was 61.9 kg (10^{th}–25^{th} centile), his height was 174.7 cm (25^{th}–50^{th} centile), and his occipital frontal circumference (OFC) was 55.5 cm (45^{th}–50^{th} centile). His anterior fontanel measured 4.5 × 3.5 cm and his posterior fontanel measured 5 × 3 cm. He had sparse, blond hair (Figures 1A and 1B). He had bitemporal prominences and closely spaced eyes. He

[1]Medical Genomics and Metabolic Genetics Branch, National Human Genome Research Institute, NIH, Bethesda, MD 20892, USA; [2]Department of Neuroscience, Mayo Clinic, Jacksonville, FL 32224, USA; [3]INSERM UMR1163, Département de Génétique, Université Paris Descartes, Sorbonne Paris Cité and Institut Imagine, Hôpital Necker – Enfants Malades, Assistance Publique – Hôpitaux de Paris, Paris 75006, France; [4]Division of Medical Genetics, School of Medicine, University of Washington, Seattle, WA 98195; [5]Dermatology, Group Health Cooperative, Seattle, WA, 98112, USA
[6]These authors contributed equally to this work
[7]These authors contributed equally to this work
*Correspondence: lesb@mail.nih.gov
http://dx.doi.org/10.1016/j.ajhg.2015.07.009.

Figure 1. Individual 1 at the Age of 29 Years
(A and B) He had sparse and blond hair, bitemporal prominences, and closely spaced eyes. He had a long nose with a convex ridge, a narrow philtrum, and retrognathia.
(C and D) He had severe contractures and shortening of his fingers and toes with small, broad, and thick toenails. The nodules and scar-like lesions on the hands, feet, and elbows reported earlier in life had resolved, although the individual had thin skin with prominent venous patterning and hyperkeratotic palms and soles with significant callus formation on the soles.

had a long nose with a convex ridge, an extremely narrow palate and philtrum, and retrognathia. He had partial eruption of four of his maxillary teeth. He had severe contractures and shortening of his fingers and toes with small, broad, and thick toenails (Figures 1C and 1D). Ophthalmology examination showed bilateral temporal and nasal corneal edema, occludable anterior segment angles, simple microphthalmia or nanophthalmos, and retinal striae with shallow orbits. The nodules and scar-like lesions had resolved, although he had thin skin with prominent venous patterning and hyperkeratotic palms and soles, with significant callus formation on the soles specifically.

Clinical testing showed moderate to severe sensorineural hearing loss. A DEXA scan demonstrated severe osteoporosis. His skeletal survey showed thin middle and lower ribs, bowed and thin tibias, diaphyseal thinning of the metacarpals and phalanges of the hands, and acro-osteolysis of the hands and feet. Head MRI demonstrated numerous arachnoid cysts with large cysts in the posterior fossa; basal ganglia calcifications were not identified on this study. Echocardiogram, electrocardiogram, and coronary artery computed tomography (CT) scan were normal.

Individual 2 was originally reported by Zufferey et al.[2] She was an adoptee of Northern Vietnamese and Chinese origin and had features similar to individual 1 that were evident by three years of age and which progressed over time. At the age of 8 years, a skin biopsy showed changes of hyperkeratosis and dermal fibrosis, with discrete areas of non-specific mononuclear inflammation, resembling keloid scarring. At age 15 she had a prematurely aged appearance, thin and sparse hair, atrophic skin with hypertrophic scarring on the knees and hands, short fingers, and flexion contractures of the fingers. Radiographs showed distal acro-osteolysis of fingers and wormian bones. Similar to individual 1, she had underdeveloped cheekbones, delayed tooth eruption and closure of the fontanels, and apparently normal intelligence.

Individual 3, the second child born to an Indonesian mother and Chinese father, was noted at birth to have macrocephaly. At 16 months of age, a head CT without contrast showed a cyst in the left posterior fossa. No basal ganglia calcifications were present. He had moderate developmental delays and received speech therapy. At 34 months of age, a karyotype, microarray, renal ultrasound, and skeletal survey were normal. MRI showed persistence of the retrocerebellar cyst.

He presented at the age of 7 years with a progressive skin abnormality reported to have begun at age 2 with several small smooth, brown bumps on the backs of his hands. These had increased in number over the years. Height and weight were both above the 50th centile; his OFC was 55 cm (95th centile). He responded appropriately to directions, but was almost mute and extremely shy during the examination.

His facial features (Figure 2A) included frontal bossing, widely spaced eyes, proptosis with loss of periorbital fat, and preservation of the buccal fat pads. He had a short nose, a convex nasal ridge, and underdeveloped cheekbones with micrognathia. His teeth were small. He had short hands and feet, broad and short distal phalanges, and thickened star-shaped scar-like lesions on the backs of his hands (Figure 2B), elbows, and knees. His skin was atrophic in other areas, particularly over his back. There was a marked vascular pattern evident on his extremities and on his trunk. His knees and elbows were disproportionately large.

A skeletal survey showed macrocephaly with dysplasia of the mandibular condyles and a small maxilla. The cheekbones were underdeveloped with absence of the nasal bone and nasal spine. There was lucency at the junction of the right frontal and right parietal bones with overlying cortical thinning and cortical expansion. The fontanels were closed. The radii and the ulnae were mildly short. The distal radius and ulna were gracile and dysplastic bilaterally. There was acro-osteolysis of all the distal phalanges and a delayed bone age. His facial features and acro-osteolysis raised the possibility of mandibuloacral dysplasia, but

Figure 2. Individual 3 at the Age of 7 Years
(A) He had distinctive facies with thin hair, sparse eyebrows, widely spaced eyes, long palpebral fissures, a narrow nasal bridge, malar flattening, and prognathism. His skin was thin.
(B) He had broad fingers with short, broad distal phalanges with hypertrophic scars.

sequencing of *LMNA* (MIM: 150330) and *ZMPSTE24* (MIM: 606480) was normal (data not shown).

At the age of 9.5 years, a skin biopsy of a new nodule showed changes of epidermal atrophy, hyperkeratosis, and dermal fibrosis. He is currently functioning below grade level with additional help in all subjects. His teacher notes that he is withdrawn in class. Formal intellectual testing was not available.

Individual 4 is of Pakistani descent and was born to distantly related parents. She presented at six months of age for "severe eczema," resulting in hospitalization. At that time her skin began to darken and poor weight and linear growth were noted. Her intellectual progress was reportedly normal. At the age of 4 years the eczema had resolved, but she had developed "wart-like" growths on her fingertips. Her weight was at the 10^{th} centile, her height at the 75^{th} centile, and her OFC was at $<2^{nd}$ centile (45.4 cm). Her anterior fontanel was open. She had proptosis and closely spaced eyes. Outer canthal and interpupillary measurements were normal. Her nasal ridge was convex, her maxilla was recessed, and she had micrognathia. She had short hands and feet with small distal phalanges. There were star-shaped scar-like lesions on her palms and horizontal linear bands of thickened skin on the dorsum of her hands and tops of her feet (Figure 3A and 3B, 6 years of age). Dermatoglyphics were absent, and there was thickened skin at the ends of the digits. She had linear areas of thickened skin with pseudopodia at the elbows and feet. Her skin was dry, but the vascular pattern was normal. A skeletal survey at age 6 showed a small maxilla and mandible, acro-osteolysis, thin long bones, and a small 12^{th} right rib and small cervical ribs.

At 14 years of age, her condition was reported to have progressed and she was no longer able to walk because of bleeding of her feet and progression of the skin thickening (Figure 3D). She had severe contractures of her fingers and toes (Figure 3C), progressive acro-osteolysis, hyperkeratotic plaques on her soles, progression of scarring on her elbows and knees, and loss of subcutaneous tissue in her extremities, giving a disproportionate, swollen appearance to her knees and elbows and a marked venous pattern on her limbs and face, along with hyperpigmentation. Her facial features had become more striking with proptosis, loss of subcutaneous tissue, and thinning of her hair. Her intellect was described as normal or above average, but no formal testing was available. She was fluent in English and Urdu. In all four probands, the family history was negative for other affected relatives.

To identify the causative variant in individual 3, exome sequencing was performed on genomic DNA isolated from him and his parents (PureGene). Solution-hybridization exome capture was performed with the Illumina TruSeq system and exome sequencing was performed with the HiSeq 2000 sequencer (Illumina). Image analyses and base calling were performed as described.[3] Reads were aligned to the NCBI Genome browser reference genome GRCh37, hg19 with Novoalign (Novocraft Technologies). Samples were sequenced to sufficient coverage such that at least 85% of the targeted exome was called with high-quality variant detection (reported as genotype at every callable position). Genotypes were called with only those sequence bases with Phred base qualities of at least Q20 via Most Probable Genotype[3] (MPG) and an MPG score of ≥ 10. Filters were applied with the VarSifter Next-Gen variant analysis software.[4] On the basis of the individuals described above, we used an autosomal-dominant mode of inheritance and the de novo trio model as the primary filter. Exome sequencing identified nine protein-coding variants that conformed to the de novo trio model and had adequate quality scores. A single variant, g.149503842A>G (c.1994T>C; p.Val665Ala [GenBank: NM_002609.3]) on chromosome 5 in *PDGFRB* (MIM: 173410), was absent in the CLINSEQ cohort of 951 individuals and was confirmed to be de novo via Sanger sequencing in both parents. The biologic parentage of the child was apparent from numerous Mendelian consistencies in the trio data. We then sequenced individuals 1, 2, and 4 for this variant and identified the same mutation in all three. To control for cross contamination, samples were tested individually as they were received in the lab, and negative controls were run with all samples. RT-PCR using primers spanning introns on total RNA isolated

Figure 3. Individual 4 at the Ages of 6 and 14 Years

She is 6 years of age in (A) and (B) and 14 years of age in (C) and (D). The views of her limbs at these two time points illustrate the severity of the progression in this individual. She had short hands and feet with small distal phalanges. There were star-shaped scar-like lesions on her palms and horizontal linear bands of thickened skin on the dorsum of her hands and tops of her feet. Dermatoglyphics were absent, and there was thickened skin at the ends of the digits. She had linear areas of thickened skin and pseudopodia of the feet. Her skin was dry, thickened, and hyperkeratotic, but the vascular pattern was normal.

from cell lines from individuals 1 and 3 also showed evidence of the mutation (RNeasy, One-Step RT-PCR, QIAGEN). In addition, the variant was not detected in either parent of individual 4, consistent with de novo occurrence. Parental samples for individuals 1 and 2 were not available. This variant was absent in the NHLBI Exome Sequencing Project dataset of 6,500 individuals and in the 61,000-sample Exome Aggregation Consortium Browser, both accessed November, 2014. We critically evaluated these genetic data[5] by estimating the statistical significance of finding the same de novo nucleotide variant in two families by chance alone. Using the three-base-context mutation-rate-prediction approach,[6] we estimate the chance of identifying this same variant in two de novo occurrences to be on the order of 10^{-16}, which is many orders of magnitude beyond genome-wide significance. That the same variant was also identified in two additional individuals (though parental samples were not available in these) would further decrease the likelihood of the null hypothesis. We conclude that these molecular genetic findings are statistically significant at a genome-wide level.[5]

We went on to functionally evaluate the predicted protein alteration in the *PDGFRB* product. We compared the function of the p.Val665Ala Penttinen syndrome variant to a loss-of-function p.Leu658Pro variant identified in individuals with idiopathic basal ganglia calcification, type 4 (IBGC4 [MIM: 615007])[7] and to wild-type PDGFRB. Human *PDGFRB* cDNA c.1973T>C (p.Leu658Pro) and wild-type pCMV constructs have been described previously.[7] The c.1994T>C (p.Val665Ala) mutation identified here was introduced independently into the wild-type *PDGFRB* pCMV construct with the QuickChange Site-Directed Mutagenesis Kit (Stratagene) and mutagenesis primers (5′-CACCTGAACGTGGcCAACCTGT TGGG-3′ [forward] and 5′-CCCAACAGGTTGgCCACGTT CAGGTG-3′ [reverse], mutation indicated in lowercase). We transfected each of the mutant and the wild-type constructs into HeLa cells. Cell culture, vector transfection, and western blotting were performed as described.[7] As expected, the wild-type construct generated three proteins detectable by an anti-PDGFRB antibody (clone 28E1, Cell Signaling Technology) and of approximately 180 kDa, 160 kDa, and 130 kDa, representing the mature, transmembrane form of the protein and two incompletely post-translationally processed forms, respectively[8] (Figure 4A, Table S1). Total PDGFRB was calculated by adding the intensity of ~180, ~160, and ~130 kDa bands. Values were normalized to α-tubulin (TUBA1A, clone DM1A; Sigma-Aldrich) to correct for loading. The 130 kDa form of the protein is minor and is not further discussed. By comparing the amount of PDGFRB that was produced by the p.Val665Ala construct to that produced by

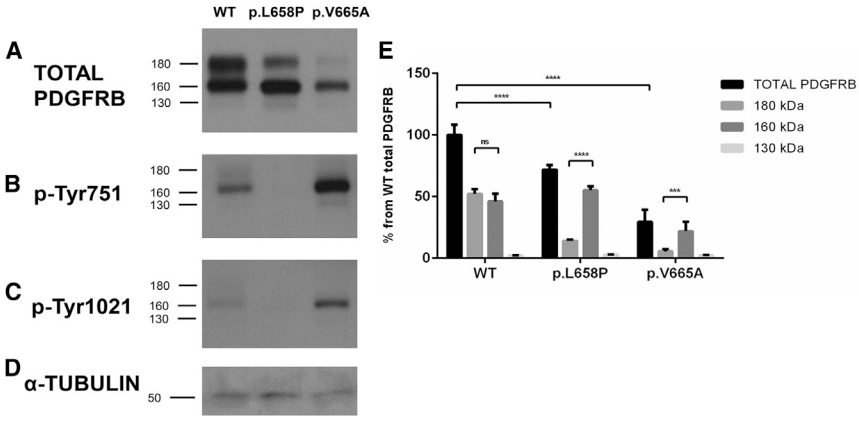

Figure 4. Expression of Total PDGFRB Receptor in HeLa Cells Transfected with WT, p.Leu658Pro, and p.Val665Ala PDGFRB Constructs

Representative western blots showing total PDGFRB (A), phosphorylated PDGFRB at tyrosine 751 (p-Tyr751) (B), and tyrosine 1021 (p-Tyr1021) (C) of the WT (wild-type), p.Leu658Pro, and p.Val665Ala variants. α-tubulin is shown as a protein loading control (D). Horizontal bars indicate the electrophoretic mobility of three mature forms of PDGFRB (180, 160, and 130 kDa) (E). Quantitative analysis of the three mature forms of total PDGFRB was observed by western blot (n = 3). Values represent the percentage (average ± S.E.M.) of each PDGFRB form from the total PDGFRB in WT cells. *** = $p < 0.001$, **** = $p < 0.0001$. ns, non-significant.

the wild-type construct, we observed that the p.Val665Ala construct generated reduced amounts of total PDGFRB with somewhat reduced absolute amounts of the 160 kDa species and very little of the mature 180 kDa form of the protein (Figures 4A and 4E). Co-transfection experiments with pEGFP-N1 (Clontech Laboratories) showed a decrease in both EGFP (anti-GFP [MAB3580]; Chemicon International) and PDGFRB in cells transfected with the p.Val665Ala construct as compared to those transfected with the wild-type PDGFRB construct (Figures S1A–S1D, n = 2). Real-time qPCR with gene-expression probes for *PDGFRB* (Hs01019589_m1) and *GAPDH* (Hs00266705_g1; LifeTechnologies) confirmed these results, showing reduced expression of *PDGFRB* in cells transfected with the p.Val665Ala construct as compared to cells transfected with the wild-type construct; mRNA was reduced by 28%, $p = 0.0007$ (Figure S1E). We are skeptical of the hypothesis that the single-nucleotide change in the construct could lead to this large of a decrease in transcription. More likely is that cells expressing high amounts of p.Val665Ala PDGFRB have reduced survival, which would result in lower apparent average total protein amounts from the transfected vectors. The phenotype demonstrated in Penttinen syndrome includes acro-osteolysis, osteoporosis, and thin skin, which is consistent with decreased cell survival. Further experiments are required to investigate this potential effect of the altered protein.

In spite of the lower overall amount of transcription associated with lower protein amounts, the p.Val665Ala Penttinen variant showed robust ligand-independent autophosphorylation when we used antibodies to Tyrosine-751 and Tyrosine-1021 (Figures 4B and 4C) in comparison to that shown by either the wild-type PDGFRB or the p.Leu658Pro IBGC variant (phospho-PDGFRβ [Tyr1021] [6F10] and phospho-PDGFRβ [Tyr751] [C63G6]; Cell Signaling Technology). We evaluated the responsiveness of the wild-type and p.Val665Ala Penttinen syndrome receptors by using transfected HeLa cells and an exogenous PDGF-BB dimer ligand (one of the natural ligands of this receptor), confirming that the p.Val665Ala construct produced greatly reduced amounts of mature 180 kDa isoform (Figure 5A). Additionally, phosphorylation of both the Tyrosine-751 and Tyrosine-1021 moieties of the 160 kDa form of the protein was greatly increased in comparison to phosphorylation in the wild-type form (Figures 5B–5D and Table S2). It was evident that the 160 kDa form of the protein was phosphorylated at both of these tyrosine residues irrespective of the presence of PDGF-BB ligand, suggesting a gain-of-function, ligand-independent hypersensitivity consequence of this mutation. Signaling through downstream effector molecules was assessed with appropriate antibodies (AKT, phospho-AKT [S473] [193H12], PLCγ1 [D9H10] XP, phospho-PLCγ1 [Tyr783] [D6M9S], SRC, phospho-SRC [pY416], phospho-Stat3 [Tyr705] [D3A7] XP, STAT3 [D3Z2G], phospho-ERK1/2 [Thr202/Tyr204] [D13.14.4E] XP, and ERK1/2 p44/42 MAPK; Cell Signaling Technology). The hyper-responsive phosphorylation of p.Val665Ala PDGFRB did not appear to be transduced via AKT, a known effector of PDGFRB signaling,[9] given that phosphorylated AKT (pAKT) was not detectably elevated in the cells transfected with the mutant construct (Figure 6A and Table S2). Because we did not see evidence of increased signal transduction from p.Val665Ala PDGFRB via pAKT, we went on to characterize other potential mediators of this signal. We surveyed a number of known mediators of this pathway, including STAT3, PLCγ1, SRC, and ERK, that have been previously found to be activated by the PDGFRB pathway.[10] Of these putative effectors, we saw evidence that both STAT3 and PLCγ1 were phosphorylated by p.Val665Ala PDGFRB in the absence of PDGF-BB (time point 0 min in Figures 6B and 6C), whereas neither SRC nor ERK showed evidence of increased signal transduction as compared that in the wild-type protein (Figures 6D and 6E).

We attempted to study the signaling attributes of this pathway in primary fibroblasts grown from skin biopsies from individuals 1 and 3. Cells were passaged in DMEM

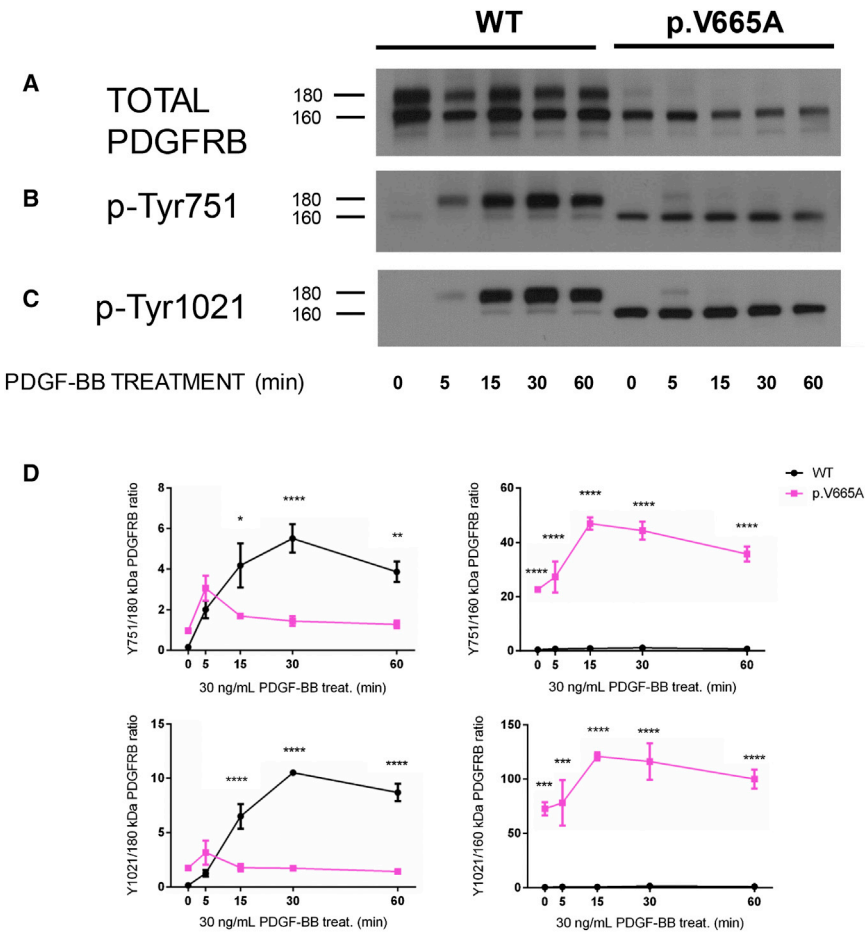

Figure 5. Time Course for the Phosphorylation of WT and p.Val665Ala PDGFRB Receptors

Representative western blots of transfected HeLa cells treated with PDGF-BB at 5, 15, 30, and 60 min and blotted to detect total PDGFRB (A), phosphorylated PDGFRB at tyrosine 751 (p-Tyr751) (B), and tyrosine 1021 (p-Tyr1021) (C). Horizontal bars indicate the electrophoretic mobility of the two main PDGFRB forms (180 and 160 kDa) (D). Schematic representation of the quantitative data obtained by western blot of the time-dependent change in the PDGF-BB-induced phosphorylation of PDGFRB ($n = 3$). Data are expressed as the fold change (average ± SEM) in p-Tyr751 and p-Tyr1021 immunoreactivity at 180 and 160 kDa bands compared to the corresponding band of total PDGFRB. * = $p < 0.05$, ** = $p < 0.01$, *** = $p < 0.001$, **** = $p < 0.0001$.

with 10% fetal bovine serum, 1% penicillin-streptomycin, 1× L-glutamine, and 2× fungizone. For stimulation experiments, cells were grown to 70% confluence in 6 cm dishes and were serum starved for 24 hr. PDGF-BB ligand (PreProtech) was added at 30 ng/ml, and cells were harvested for protein. Cells were lysed by a 10 min incubation in 200 ul of 1× cell lysis buffer (eBioscience) with the addition of enhancer solution (eBioscience), and proteins were separated on 8%–16% Tris-Glycine gels (Life Technologies). Proteins were transferred to nitrocellulose (iBlot system, Life Technologies). An additional antibody directed against phospho-PDGFRB (Tyr751) (88H8) was used for these experiments (Cell Signaling Technology).

We did not see evidence of phosphorylation of the 160 kDa form of the receptor in either of these cell lines, and there was no evidence of phosphorylation without ligand stimulation (data not shown). Ligand-induced phosphorylation of the 180 kDa form of the receptor was seen in both mutant and control fibroblasts. No apparent difference was noted between control and mutant fibroblasts in either the absolute amount of PDGFRB or the phosphorylation of the 180 kDa form of the receptor. Expression of the mutant allele was confirmed by RT-PCR followed by Sanger sequencing. It is possible that either phosphorylation of this form of the receptor is at amounts too low to be detected by this assay or the receptor is degraded or unstable when produced at natural (as opposed to overproduction in transient transfection models) amounts in the heterozygous state. Alternatively, it is possible that skin fibroblasts are not the appropriate cell type for studying the effect of this *PDGFRB* mutation. Immunohistochemistry may allow differences to be seen in cells other than fibroblasts, and future studies are planned to address this question.

PDGFRB (the platelet-derived growth factor receptor β) is a homodimeric type-III tyrosine-kinase receptor that binds several ligands, but the physiologically relevant ligand for this receptor is the PDGF-BB homodimer. This ligand-receptor pair is involved in processes of wound healing, sclerotic diseases, and tumor angiogenesis, among others.[9,11,12] Mutations in *PDGFRB* have previously been implicated in three distinct disorders. Loss-of-function mutations in *PDGFRB* cause IBGC4.[7,13,14] Predicted gain-of-function mutations have been associated with autosomal-dominant infantile myofibromatosis (MIM: 228550),[15,16] which has no overlapping features with IBGC4. Recently, Takenouchi et al.[17] described two individuals with a distinctive phenotype of skeletal overgrowth, dysmorphic features, and neurobehavioral manifestations caused by a recurrent, apparently de novo c.1751C>G p.Pro584Arg variant in *PDGFRB*. We conclude that Penttinen syndrome is allelic to IBGC4, infantile myofibromatosis, and the syndrome described by Takenouchi et al.[17]

The four individuals described here had proptosis, a convex nasal bridge, underdeveloped cheekbones, delayed closure of the fontanels, delayed tooth eruption,

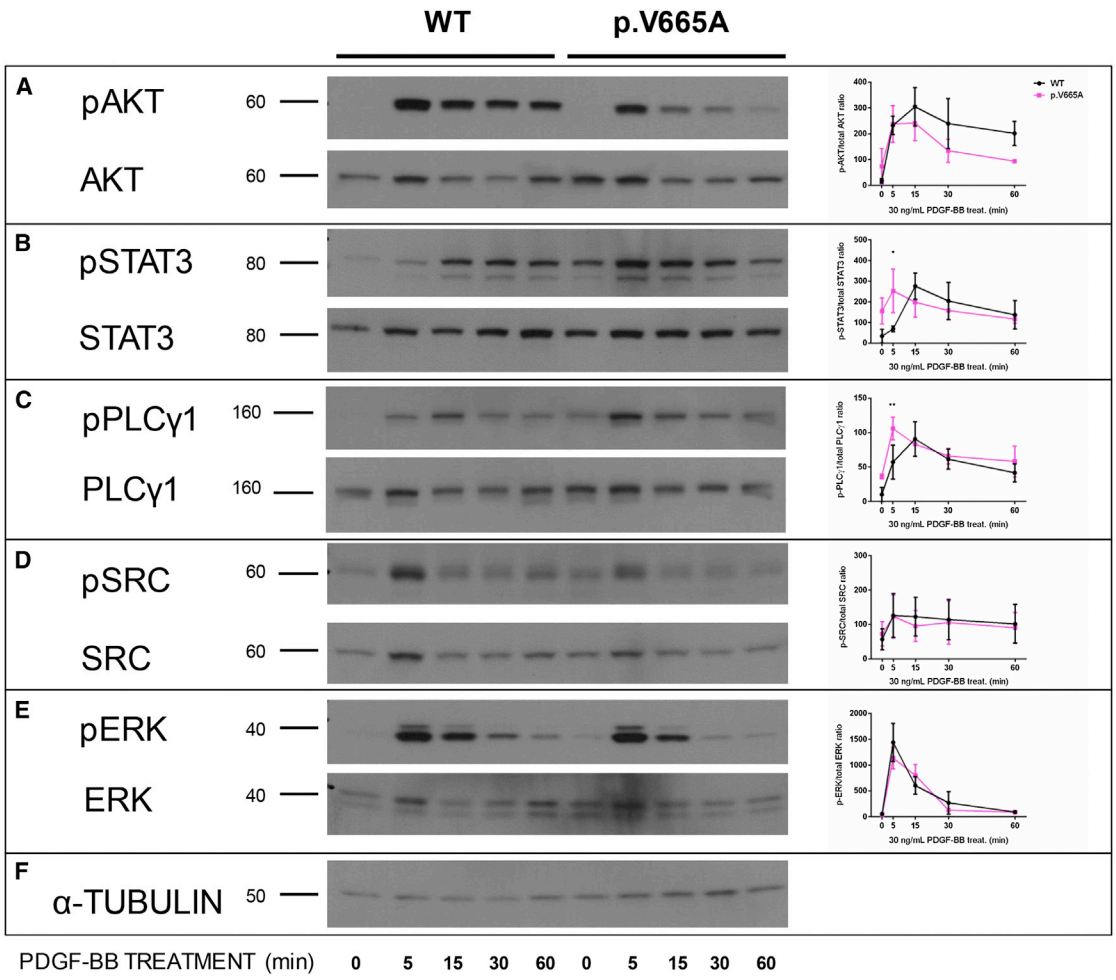

Figure 6. Time Course for the Phosphorylation of PDGFRB Downstream Signaling Molecules in HeLa Cells Transfected with WT and p.Val665Ala Constructs

Representative western blots of transfected HeLa cells treated with PDGF-BB at 5, 15, 30 and 60 min blotted to detect phosphorylated AKT (pAKT) and total AKT (A), phosphorylated STAT3 (pSTAT3) and total STAT3 (B), phosphorylated PLCγ1 (pPLCγ1) and total PLCγ1 (C), phosphorylated SRC (pSRC) and total SRC (D), and phosphorylated ERK (pERK) and total ERK (E). α-tubulin is shown as a protein loading control (F). Molecular size is indicated in kDa. A schematic representation of the quantitative data obtained by western blot of the time-dependent change in the PDGF-BB-induced phosphorylation of AKT, STAT3, PLCγ1, SRC, and ERK is shown at the right of the corresponding blots (n = 3). Data are expressed as the fold change (average ± SEM) in pAKT, pSTAT3, pPLCγ1, pSRC, and pERK in comparison to total AKT, STAT3, PLCγ, SRC, and ERK, respectively. * = $p < 0.05$, ** = $p < 0.01$.

progressive cutaneous atrophy and hypertrophic skin lesions, and skeletal changes, including acro-osteolysis (Table 1). It is striking to us that the hypertrophic skin changes in the four individuals described here are not myofibromas; that, although there are CNS findings in these individuals, they do not include basal ganglia calcifications; and that, whereas the individuals described by Takenouchi et al.[17] were described as having thin and fragile skin, their facial features, skeletal changes, and cognitive-psychiatric features were distinct from the individuals described here. These four conditions show very little phenotypic overlap with each other, and we conclude that the disorder manifested in the four individuals described here is distinct and should be called Penttinen syndrome.

There are little genetic or functional data upon which to develop models of pathogenesis that explain the phenotype heterogeneity of these four *PDGFRB*-related disorders. The mutational spectrum of the four disorders is limited to eight amino acid substitutions (Figure S2). All lie in the carboxy-terminal half of the predicted protein, which includes the kinase domain. We were unable to discern any pattern or relationship of mutation position to phenotype. Published data on the functional consequences of *PDGFRB* variants are only available for some of the variants associated with IBGC4. It has been proposed that the *PDGFRB* variants associated with infantile myofibromatosis are activating, based on bioinformatic modeling.[16] Indeed, some preliminary evidence to this effect has been presented (Drs. K. Oishi, B.R. Evans, and J.A. Martignetti, personal communication). We are unaware of any published functional data for the mutation associated with the syndrome described by Takenouchi et al.[17] Several *PDGFRB* mutations associated with IBGC4 have been shown to cause a reduction in the mature, transmembrane form of PDGFRB and a

Table 1. Major Clinical Findings in Four Individuals with Penttinen Syndrome as Compared to Clinical Findings in Three Distinct Disorders Caused by Mutations in *PDGFRB*

	Individual 1 (Penttinen et al., 1997)	Individual 2 (Zufferey et al., 2013)	Individual 3	Individual 4	Penttinen Syndrome	Kosaki Syndrome (Takenouchi et al., 2015)	Infantile Myofibromatosis	Idiopathic Basal Ganglia Calcification
Age (at last evaluation)	**29 years**	**15 years**	**7 years**	**14 years**	**NA**	**14 years, 17 years[a]**	**NA**	**NA**
Craniofacial								
Open fontanelles	+	+	−	+	+	−	−	−
Shallow orbits	+	+	+	+	+	−	−	−
Narrow nose	+	−	+	+	+	−	−	−
Underdeveloped cheekbones	+	+	+	+	+	−	−	−
Delayed eruption of teeth	+	+	+	+	+	NS	−	−
Ophthalmologic								
Microphthalmia	+	NS	NS	NS	+ (?)	NS	−	−
Corneal abnorm	+	NS	NS	NS	+ (?)	NS	−	−
Dermatologic								
Thin, translucent skin with prominent venous patterning	+	+	+	+	+	+	−	−
Lipoatrophy	+	+	+	+	+	−	−	−
Hyperkeratotic lesions	+	+	+	+	+	−	−	−
Sparse hair	+	+	+	+	+	−	−	−
Skeletal								
Acro-osteolysis	+	+	+	+	+	−	−	−
Short fingers	+	+	+	+	+	−	−	−
Contractures	+ (fingers, toes)	+ (fingers)	+ (fingers)	+ (fingers)	+ (fingers, toes)	−	−	−
Osteopenia	+	+	+	+	+	−	−	−
Thin bones	+	+	+	+	+	−	−	−
Scoliosis	+	−	−	−	−/+	+	−	−
Skull	thin calvarium	wormian bones	thin calvarium	thin calvarium	thin calvarium	diffuse granular pattern	−	−
Neurological								
Cognitive ability	Nl	Nl	DD	NI	NI	NI, DD	NI	Abnl
Hearing loss	B SNHL	−	−	−	−	NA	−	−
Brain malformation	mega cisterna magna, other	cortical and cerebellar atrophy	posterior fossa cyst	NA	+/−	extensive periventricular white matter lesions	−	basal ganglia calcifications
Other								
Thyroid abnorm	hypothyroid	NS	NS	NS	+ (?)	NS	−	−
Hyperextensible	+	+	+	+	+	−	−	−

(*Continued on next page*)

Table 1. *Continued*

	Individual 1 (Penttinen et al., 1997)	Individual 2 (Zufferey et al., 2013)	Individual 3	Individual 4	Penttinen Syndrome	Kosaki Syndrome (Takenouchi et al., 2015)	Infantile Myofibromatosis	Idiopathic Basal Ganglia Calcification
Age (at last evaluation)	**29 years**	**15 years**	**7 years**	**14 years**	**NA**	**14 years, 17 years[a]**	**NA**	**NA**
Distinguishing Features of PDGFRB Disorders Other than Penttinen Syndrome								
Overgrowth	–	–	–	–	–	+	–	–
Myofibromas	–	–	–	–	–	+	+	–
Basal ganglia calcifications	–	–	–	–	–	–	–	+

Abbreviations are as follows: +, positive for; –, negative for; Abnl, abnormal intelligence; NI, normal intelligence; DD, developmental delay; NA, not applicable; NS, not assessed; B SNHL, bilateral sensorineural hearing loss; (?), not enough information to be certain.
[a]Only two individuals have been described with this condition and these are their ages.

reduction of signal transduction via phosphorylation of the two well-studied tyrosine moieties of this protein.[7,10] It is reasonable to conclude that IBGC4 is caused by a reduced signal-transduction capacity of this protein.

To understand the distinct clinical consequences of the Penttinen syndrome mutation, we performed a functional analysis of this variant and compared it to the p.Leu658Pro variant that causes IBGC4. We have shown that the Penttinen syndrome variant shows a gain of function through phosphorylation of tyrosine residues on the 160 kDa form in the absence of ligand. We conclude from these data that the Penttinen syndrome variant is a gain-of-function mutation leading to excess, ligand-independent phosphorylation.

Both Penttinen syndrome and myofibromatosis appear to be caused by gain-of-function mutations. There are a substantial number of downstream effectors of signal transduction from receptor tyrosine kinases. We show evidence that the effectors of the p.Val665Ala PDGFRB Penttinen syndrome variant appear to include STAT3 and PLCγ1. Although mutations in *PLCG1* have not been associated with disease, activating mutations in *STAT3* are known to be involved in cancer and autoimmune disease. Additionally, STAT3 is thought to have a role in keloid formation given that inhibitors of STAT3 phosphorylation in keloid fibroblasts suppress increased collagen production, proliferation, and migration.[18] The individuals presented here have hypertrophic skin lesions, and it is possible that activation of STAT3 plays a role in these lesions. However, further studies are needed to confirm the involvement of these two effectors in the etiology of Penttinen syndrome. We hypothesize that distinct gain-of-function mutations in *PDGFRB* transduce aberrant signals through other effectors, or combinations of effectors, that are responsible for the heterogeneous phenotypes associated with mutations in this gene. Given the currently restricted spectrum of mutations in *PDGFRB*, we predict that there will be other distinct phenotypes associated with mutations in this gene, that these mutations will be associated with heterogeneous signal-transduction effects, and that these disorders have much to teach us about normal and abnormal signal transduction in growth, development, and many other processes of health and disease. These data provide hints about therapeutic approaches that may be used to treat disorders caused by *PDGFRB* mutations. For Penttinen syndrome, drugs that inhibit PDGFRB or the downstream effectors are rational therapeutic candidates.

Supplemental Data

Supplemental Data include two tables and two figures and can be found with this article online at http://dx.doi.org/10.1016/j.ajhg.2015.07.009.

Acknowledgments

This work was supported by the Intramural Research Program of the National Human Genome Research Institute of the NIH and by the National Institute of Neurological Disorders and Stroke grant P50 NS072187. The authors are grateful to the individuals and their families for their support and cooperation in this work. We thank Dr. Brian Brooks and Dr. Thomas Darling for their involvement and help with individual 1, Dr. Judith Martin for her involvement and help with individual 4, Dr. Heather Brandling-Bennett for her involvement and help with individual 3, Dr. Raj Kapur for his help with interpretation of the biopsy of individual 3, Dr. Maila Penttinen for contact information for individual 1, and Dr. Yujun Han for the mutation-rate-prediction analysis. We thank Drs. Pamela Schwartzberg and Harold Varmus for advice and critical evaluation of the functional data. We thank Julia Fekecs for graphic-design support. The authors thank the Exome Aggregation Consortium and the groups that provided exome-variant data for comparison. L.G.B. is an uncompensated advisor to Illumina and receives royalties from Genentech.

Received: May 15, 2015
Accepted: July 21, 2015
Published: August 13, 2015

Web Resources

The URLs for data presented herein are as follows:

CLINSEQ, http://www.genome.gov/20519355

ExAC Browser, http://exac.broadinstitute.org/
NCBI Genome, http://www.ncbi.nlm.nih.gov/gene
NHLBI Exome Sequencing Project (ESP) Exome Variant Server, http://evs.gs.washington.edu/EVS/
OMIM, http://www.omim.org/

References

1. Penttinen, M., Niemi, K.M., Vinkka-Puhakka, H., Johansson, R., and Aula, P. (1997). New progeroid disorder. Am. J. Med. Genet. *69*, 182–187.
2. Zufferey, F., Hadj-Rabia, S., De Sandre-Giovannoli, A., Dufier, J.L., Leheup, B., Schweitze, C., Bodemer, C., Cormier-Daire, V., and Le Merrer, M. (2013). Acro-osteolysis, keloid like-lesions, distinctive facial features, and overgrowth: two newly recognized patients with premature aging syndrome, Penttinen type. Am. J. Med. Genet. A. *161A*, 1786–1791.
3. Teer, J.K., Bonnycastle, L.L., Chines, P.S., Hansen, N.F., Aoyama, N., Swift, A.J., Abaan, H.O., Albert, T.J., Margulies, E.H., Green, E.D., et al.; NISC Comparative Sequencing Program (2010). Systematic comparison of three genomic enrichment methods for massively parallel DNA sequencing. Genome Res. *20*, 1420–1431.
4. Teer, J.K., Green, E.D., Mullikin, J.C., and Biesecker, L.G. (2012). VarSifter: visualizing and analyzing exome-scale sequence variation data on a desktop computer. Bioinformatics *28*, 599–600.
5. MacArthur, D.G., Manolio, T.A., Dimmock, D.P., Rehm, H.L., Shendure, J., Abecasis, G.R., Adams, D.R., Altman, R.B., Antonarakis, S.E., Ashley, E.A., et al. (2014). Guidelines for investigating causality of sequence variants in human disease. Nature *508*, 469–476.
6. Allen, A.S., Berkovic, S.F., Cossette, P., Delanty, N., Dlugos, D., Eichler, E.E., Epstein, M.P., Glauser, T., Goldstein, D.B., Han, Y., et al.; Epi4K Consortium; Epilepsy Phenome/Genome Project (2013). De novo mutations in epileptic encephalopathies. Nature *501*, 217–221.
7. Sanchez-Contreras, M., Baker, M.C., Finch, N.A., Nicholson, A., Wojtas, A., Wszolek, Z.K., Ross, O.A., Dickson, D.W., and Rademakers, R. (2014). Genetic screening and functional characterization of PDGFRB mutations associated with basal ganglia calcification of unknown etiology. Hum. Mutat. *35*, 964–971.
8. Keating, M.T., and Williams, L.T. (1987). Processing of the platelet-derived growth factor receptor. Biosynthetic and degradation studies using anti-receptor antibodies. J. Biol. Chem. *262*, 7932–7937.
9. Demoulin, J.B., and Essaghir, A. (2014). PDGF receptor signaling networks in normal and cancer cells. Cytokine Growth Factor Rev. *25*, 273–283.
10. Arts, F.A., Velghe, A.I., Stevens, M., Renauld, J.C., Essaghir, A., and Demoulin, J.B. (2015). Idiopathic basal ganglia calcification-associated PDGFRB mutations impair the receptor signalling. J. Cell. Mol. Med. *19*, 239–248.
11. Iwayama, T., and Olson, L.E. (2013). Involvement of PDGF in fibrosis and scleroderma: recent insights from animal models and potential therapeutic opportunities. Curr. Rheumatol. Rep. *15*, 304.
12. Barrientos, S., Stojadinovic, O., Golinko, M.S., Brem, H., and Tomic-Canic, M. (2008). Growth factors and cytokines in wound healing. Wound Repair Regen. *16*, 585–601.
13. Hayashi, T., Legati, A., Nishikawa, T., and Coppola, G. (2015). First Japanese family with primary familial brain calcification due to a mutation in the PDGFB gene: an exome analysis study. Psychiatry Clin. Neurosci. *69*, 77–83.
14. Nicolas, G., Pottier, C., Charbonnier, C., Guyant-Maréchal, L., Le Ber, I., Pariente, J., Labauge, P., Ayrignac, X., Defebvre, L., Maltête, D., et al.; French IBGC Study Group (2013). Phenotypic spectrum of probable and genetically-confirmed idiopathic basal ganglia calcification. Brain *136*, 3395–3407.
15. Martignetti, J.A., Tian, L., Li, D., Ramirez, M.C., Camacho-Vanegas, O., Camacho, S.C., Guo, Y., Zand, D.J., Bernstein, A.M., Masur, S.K., et al. (2013). Mutations in PDGFRB cause autosomal-dominant infantile myofibromatosis. Am. J. Hum. Genet. *92*, 1001–1007.
16. Cheung, Y.H., Gayden, T., Campeau, P.M., LeDuc, C.A., Russo, D., Nguyen, V.H., Guo, J., Qi, M., Guan, Y., Albrecht, S., et al. (2013). A recurrent PDGFRB mutation causes familial infantile myofibromatosis. Am. J. Hum. Genet. *92*, 996–1000.
17. Takenouchi, T., Yamaguchi, Y., Tanikawa, A., Kosaki, R., Okano, H., and Kosaki, K. (2015). Novel overgrowth syndrome phenotype due to recurrent de novo PDGFRB mutation. J. Pediatr. *166*, 483–486.
18. Lim, C.P., Phan, T.T., Lim, I.J., and Cao, X. (2006). Stat3 contributes to keloid pathogenesis via promoting collagen production, cell proliferation and migration. Oncogene *25*, 5416–5425.

The American Journal of Human Genetics

Supplemental Data

A Point Mutation in *PDGFRB* Causes Autosomal-Dominant Penttinen Syndrome

Jennifer J. Johnston, Monica Y. Sanchez-Contreras, Kim M. Keppler-Noreuil, Julie Sapp, Molly Crenshaw, NiCole A. Finch, Valerie Cormier-Daire, Rosa Rademakers, Virginia P. Sybert, and Leslie G. Biesecker

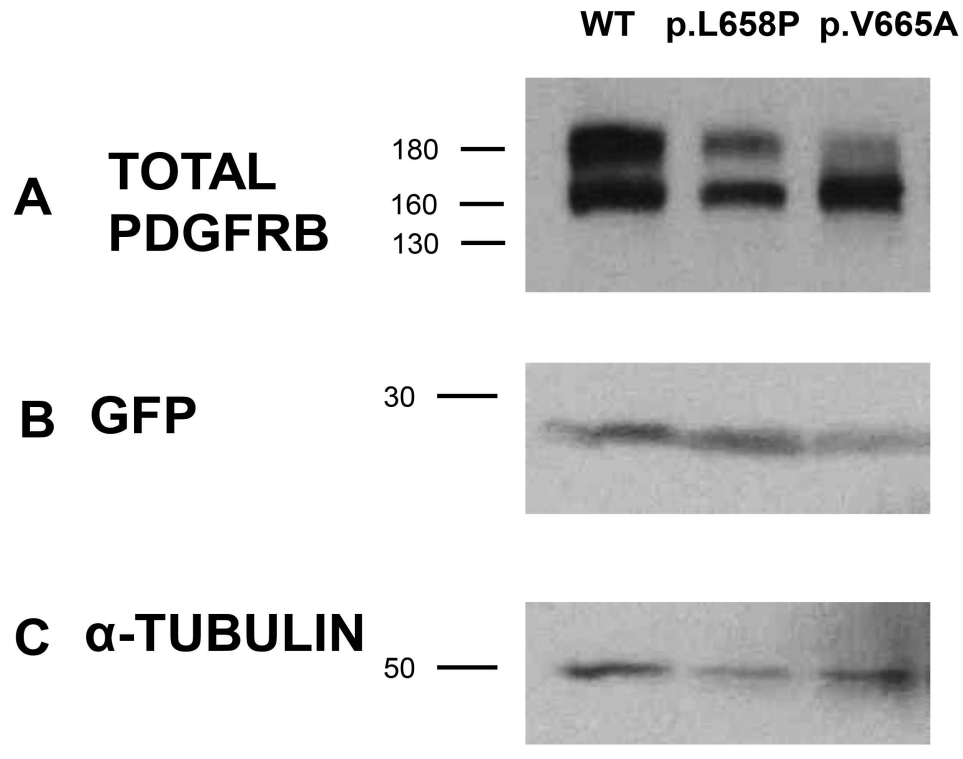
WT p.L658P p.V665A
A
TOTAL PDGFRB
180
160
130
B GFP
30
C α-TUBULIN
50

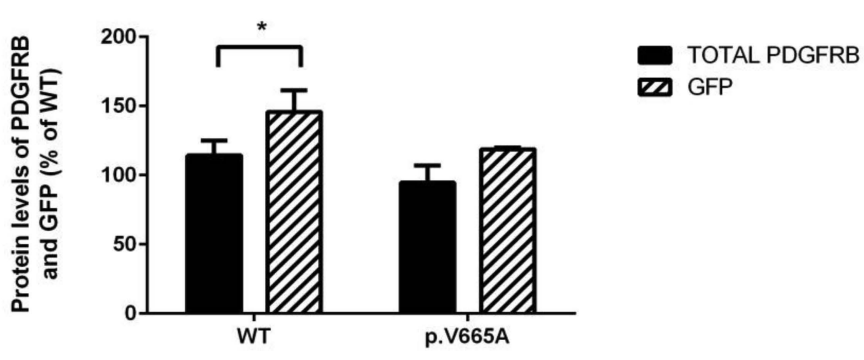
D
Protein levels of PDGFRB and GFP (% of WT)
200
150
100
50
0
*
WT
p.V665A
TOTAL PDGFRB
GFP

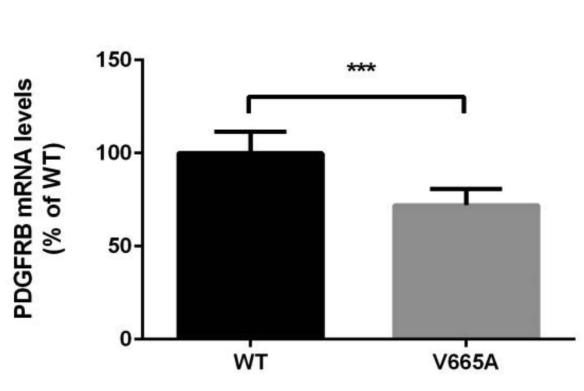
E
PDGFRB mRNA levels (% of WT)
150
100
50
0
***
WT
V665A

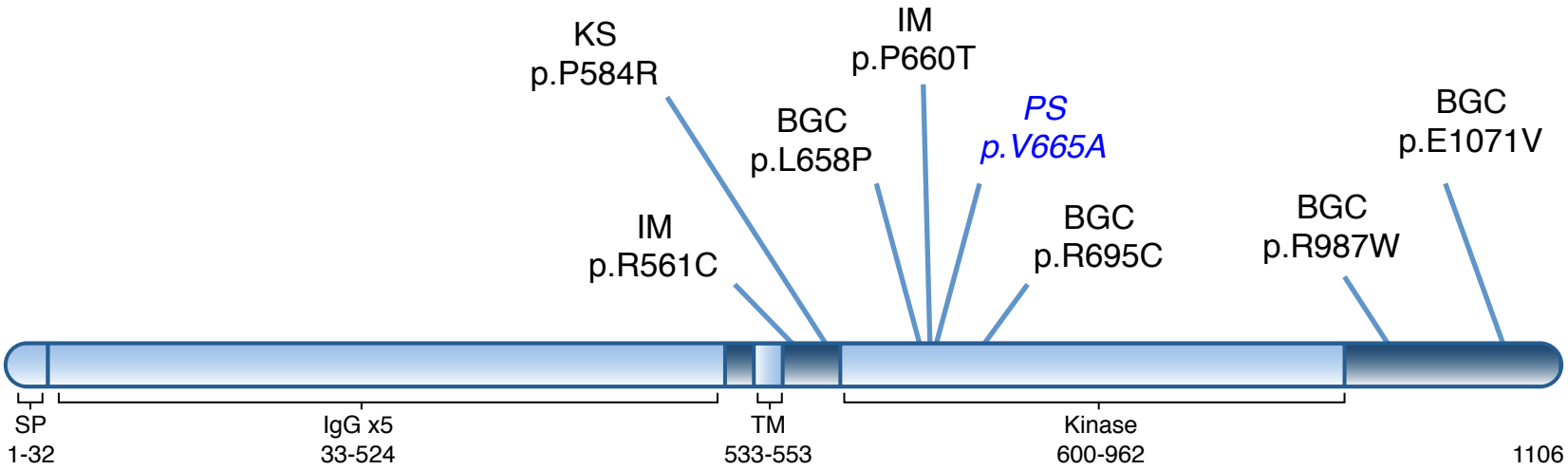

Variant	Disease	ExAC alleles*	Cellular Effect
p.Arg561Cys	Infantile myofibromatosis	0	Unknown
p.Pro584Arg	Kosaki syndrome	0	Unknown
p.Leu658Pro	Basal ganglia calcification	0	Reduced protein levels, no phosphorylation with PDGFR-BB stimulation
p.Pro660Thr	Infantile myofibromatosis	1	Unknown
p.Val665Ala	Penttinen syndrome	0	Reduced protein levels, phosphorylation in absence of ligand, predominant species is immature 160kD
p.Arg695Cys	Basal ganglia calcification	10	Reduced protein levels, reduced phosphorylation with PDGFR-BB stimulation
p.Arg987Trp	Basal ganglia calcification	2	Reduced protein levels
p.Glu1071Val	Basal ganglia calcification	0	Unknown

*Approximately 120,000 alleles were screened for each variants with the exception of p.Glu1071Val, for this variant approximately 85,000 alleles were screened.

Fig S1. Co-transfection Efficiency and mRNA Expression studies of mutant vectors. Representative western blots showing total levels of PDGFRB (A), GFP (B) and α−tubulin (C). Quantitative analysis of total PDGFRB and GFP observed by western blot (n=2) (D). Difference in protein level between wild-type and pVal665Ala construct was not found to be significant. Expression level of *PDGFRB* in cells transfected with wild-type or p.Val665Ala construct (E). p.Val665Ala construct was determined to express 28% less *PDGFRB* mRNA (P=0.0007, n=6).

Fig. S2. Location of Mutations Identified in PDGFRB. Eight mutations have been identified in *PDGFRB* in individuals with four distinct phenotypes. Protein alterations and corresponding phenotypes are shown above the protein model (IM, Infantile myofibromatosis; KS, Kosaki syndrome; BGC, Basal ganglia calcification; PS, Penttinen syndrome). Protein domains are indicated below the protein model and include the signal peptide (SP), extracellular immunoglobulin-like domains (IgG), trans membrane domain (TM) and split tyrosine-kinase domain. Allele counts for each variant as reported in ExAC and cellular effect if known are summarized in the table.

Table S1. Quantitative analysis of the three maturation forms of total PDGFRB observed by Western Blot. The percentage of the each PDGFRB band was calculated from the total PDGFRB in WT.

PDGFRB form	WT (n=3)	p.L658P (n=3)	p.V665A (n=3)
Total PDGFRB	100.0%	71.8% ±1.9 (**<0.0001**)	29.4% ±5 (**<0.0001**)
180 kDa	52.1% ±2	14.0% ±0.6	5.5% ±0.9
160 kDa	45.9% ±3.2	55.1% ±1.6	21.8% ±3.9
Ratio of 180 kDa/160 kDa forms	1.1	0.3 (**<0.0001**)	0.3 (**<0.0001**)

(Significant P values for difference between WT and mutant protein.)

Table S2. Quantification of the time-dependent change in the PDGF-BB induced phosphorylation of PDGFRB and downstream pathways. Data is expressed as the fold change (average ± S.E.M.) in p-Tyr751 PDGFRB, p-Tyr1021 PDGFRB, pAKT, pSTAT3, pPLCγ1, pSRC and pERK immunoreactivity compared to total PDGFRB, AKT, STAT3, PLCγ1, SRC and ERK respectively.

	PDGF-BB Time Course				
	0 min (n=3)	**5 min** (n=3)	**15 min** (n=3)	**30 min** (n=3)	**60 min** (n=3)
PDGFRB p-Tyr751/180					
WT	0.2 ± 0.1	2 ± 0.4	4.2 ± 1.1	5.5 ± 0.7	3.9 ± 0.5
V665A	1 ± 0.2	3.1 ± 0.6	1.7 ± 0.1 **(<0.05)**	1.4 ± 0.2 **(<0.0001)**	1.3 ± 0.2 **(<0.01)**
PDGFRB p-Tyr751/160					
WT	0.4 ± 0.1	0.7 ± 0.2	0.9 ± 0.3	1.1 ± 0.2	0.7 ± 0.1
V665A	22.6 ± 1.2 **(<0.0001)**	27.3 ± 5.8 **(<0.0001)**	47 ± 2.3 **(<0.0001)**	44.4 ± 3.4 **(<0.0001)**	35.7 ± 2.8 **(<0.0001)**
PDGFRB p-Tyr1021/180					
WT	0.1 ± 0.1	1.3 ± 0.3	6.5 ± 1.1	10.5 ± 0.1	8.7 ± 0.8
V665A	1.7 ± 0.2	3.2 ± 1.1	1.8 ± 0.3 **(<0.0001)**	1.7 ± 0.2 **(<0.0001)**	1.4 ± 0.2 **(<0.0001)**
PDGFRB p-Tyr1021/160					
WT	0.5 ± 0.2	0.9 ± 0.1	0.7 ± 0.3	1.5 ± 0.4	1 ± 0.2
V665A	72.6 ± 6.2 **(<0.001)**	78.2 ± 21 **(<0.001)**	121 ± 3.8 **(<0.0001)**	116.2 ± 16.7 **(<0.0001)**	100.1 ± 8.6 **(<0.0001)**
p-AKT					
WT	17.2 ± 5	232 ± 20.7	304.4 ± 43.6	239.6 ± 56.1	201.6 ± 27
V665A	73.7 ± 40	237.6 ± 41	241.5 ± 39.7	134.4 ± 25.8	93.8 ± 3
p-STAT3					
WT	34.4 ± 19.3	69 ± 7.7	276.2 ± 44.8	204 ± 51.8	137 ± 39.7
V665A	155.6 ± 36.3	253.1 ± 60.8 **(<0.05)**	198.3 ± 42.2	157.8 ± 26.3	116.6 ± 12.2
p-PLCγ1					
WT	10.2 ± 6	57.2 ± 14.3	90.6 ± 14.6	61.5 ± 8.4	41.7 ± 7.6
V665A	36.3 ± 1.8	106 ±9.5 **(<0.01)**	83.1 ± 1.1	65.9 ± 6.6	58.3 ± 13
p-SRC					
WT	57.1 ± 17.8	125.9 ± 36.8	122.7 ± 32.4	114.2 ± 33.7	101.7 ± 32.7
V665A	72.9 ± 20.2	123.6 ± 36.1	95.7 ± 26.2	105.7 ± 36.4	90.6 ± 25.2
pERK					
WT	56.2 ± 16.3	1437 ± 261.3	604.9 ± 119.5	269.9 ± 127.7	90.2 ± 20.6
V665A	38.4 ± 10.7	1136 ± 119.7	801.2 ± 123.5	129 ± 20.5	87.2 ± 8